FED-Vol. 190, Cavitation and Gas-Liquid Flow
in Fluid Machinery and Devices
ASME 1994

ON THE DYNAMICS AND ACOUSTICS OF CLOUD CAVITATION ON AN OSCILLATING HYDROFOIL

E. A. McKenney and Christopher E. Brennen
Department of Mechanical Engineering
California Institute of Technology
Pasadena, California

ABSTRACT

Observations have been made of the growth and collapse of surface and cloud cavitation on a finite aspect ratio hydrofoil oscillating in pitch. The cavitation was recorded using both still and high-speed motion picture photography, and the variations with cavitation number and reduced frequency of oscillation were investigated. The noise generated by the cavity collapse was also measured and analyzed. The acoustic signals associated with individual cavity collapse events have been synchronized with the motion pictures, providing insights into the correspondence between the flow structures involved in the cavity collapse process and the sound generated by them.

INTRODUCTION

Cavitation occurring on lifting surfaces has received a great deal of attention due to its detrimental characteristics, such as erosion damage to the surface and the generation of noise. Previous studies have considered the causes and character of the inception of such cavitation, the mechanisms which cause the most severe erosion, and the correlation of the flow mechanisms with the noise produced when they collapse. In particular it has been noted that, as an attached cavity collapses and is shed into the wake, the breakup of the cavity often results in the occurrence of cloud cavitation. The structure of such clouds appears to contain strong vortices, perhaps formed by the shear layer at the surface of the collapsing cavity (Kubota, et al., 1989; Maeda, et al., 1991); these clouds then collapse with some violence, often causing severe erosion on the surface and generating significant amounts of noise (Bark and van Berlekom, 1978; Kato, 1985; Ye, et al., 1989; Soyama, et al., 1992). Some of the research has been primarily concerned with stationary foil sections in a constant freestream, but consideration has also been given to the effect of an unsteady flow environment, and to the effects of finite span (Shen and Peterson, 1978; Shen and Peterson, 1980; Franc and Michel, 1988; Hart, et al., 1990; Kato, et al., 1992).

The present study is based on experiments performed in the Low Turbulence Water Tunnel at the California Institute of Technology. In order to gain an understanding of the flow mechanisms that produce the cavitation noise, acoustic measurements from the cavity collapse were correlated with high-speed motion pictures of cavitation on the foil.

EXPERIMENTAL SETUP

The Caltech Low Turbulence Water Tunnel (LTWT) is a closed-circuit facility, with a $30.5cm$ x $30.5cm$ x $2.5m$ test section and a 16:1 contraction ratio. It is capable of freestream velocities up to $10m/s$ and can support pressures down to $20kPa$. It is equipped with a $5\mu m$ filtration system, and a deaeration system capable of reducing the dissolved air content of the water to $3ppm$. Gates [1977] provides a complete description of this facility.

An NACA 64A309 hydrofoil was reflection-plane mounted in the test section, as shown in Figure 1 and described in Hart, et al. [1990]. The hydrofoil has a

rectangular planform with an 15.2*cm* chord length, and a span of 17.5*cm*. This foil, constructed out of stainless steel, is polished to a smooth finish. The hydrofoil is connected to a 750 watt DC motor by a four-bar linkage such that it oscillates nearly sinusoidally in pitch about a point near the center of pressure, x/c=0.38. A slip-collet connecting the oscillation linkage to a coupling shaft allows adjustment of the mean angle of attack. In addition, the oscillation linkage is adjustable for oscillation amplitudes ranging from $\pm 1^{o}$ to $\pm 5^{o}$. The oscillation rate is adjustable from 0 to 50*Hz*. An optical shaft encoder mounted to the DC motor provides a digital signal (1024 pulses per revolution) which was used to synchronize acoustic measurements with the phase of the foil.

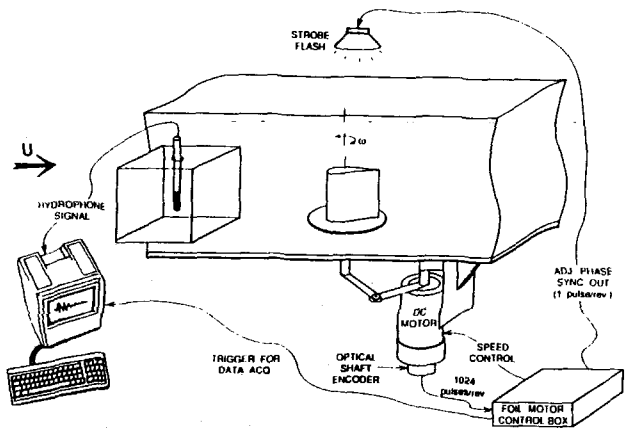

FIGURE 1. OSCILLATING HYDROFOIL FLOW VISUALIZATION SETUP.

The sound generated by the cavitation was recorded using a B&K model 8103 hydrophone (bandwidth 100kHz), installed in a Lucite box filled with water and affixed tightly to the side of the test section in order to best couple the hydrophone response to the pressure fluctuations in the test section. As graphically demonstrated by Bark and van Berlekom [1978], isolating the hydrophone in this manner significantly degrades the signal. On the other hand, it is a simple way to obtain preliminary data. The hydrophone output signal was amplified and then recorded by a PC, along with timing information from the oscillation of the foil. Still photographs were taken of various stages of the cavitation process by using the foil timing to trigger strobe lights at the desired phase of the foil oscillation cycle. A high speed (500 frames per second) 16mm movie camera was also used to film several complete oscillation cycles under selected conditions. A special circuit was designed to record foil timing information on the edge of the movie film, as well as to indicate the moment at which acoustic data was recorded during filming. This allowed later synchronization of the acoustic signals with the details of the cavitation process.

Acoustic data was also collected from the water tunnel test section without cavitation, for the purpose of eliminating any facility resonances from the cavitation data. It was determined that most of the tunnel impulse response appeared at very low frequencies. Since most of the distinctive features of the cavitation data are high-frequency bursts, the data was filtered using a digital high-pass filtering algorithm with a cutoff frequency of 500 Hz.

The high-speed motion pictures were used to obtain information about the cavitation process itself. The film was projected onto a grid, and the area covered by the cavity in a given frame was measured and normalized by the area covered by the foil surface. Certain distinctive events in the cavitation sequence were also noted, such as the moment of tip vortex cavity inception and the beginning of the collapse phase. The angle of the foil during each frame was calculated from the location of the marks on the film. Since each angle of attack between α=0° and α=10° is visited twice by the foil during a single oscillation cycle, the results are presented here in terms of *phase angle*. The phase angle, ϕ, is defined such that ϕ=0° represents α=0°, ϕ=180° indicates α=10°, and ϕ=360° means the foil has returned to α=0°. Thus from ϕ=0° to ϕ=180° the angle of attack is increasing, and from ϕ=180° to ϕ=360° the angle of attack is decreasing.

For the two reduced frequencies represented by the motion pictures, 500 frames per second results in a phase angle resolution of 8.3° (for k=0.74 cases) or 6.3° (for k=0.56) between frames.

CLOUD CAVITATION FORMATION

Figure 2 demonstrates how, for one particular set of flow conditions, the cavity size changes during one oscillation cycle. Also displayed are letters which indicate the average phase angles at which certain identifiable events were seen to occur. These events are best identified by the following chronology, which is illustrated schematically in Figure 3 and photographically in Figure 10. As the phase angle increases from ϕ=0° and reaches about ϕ=100° (point A), the tip vortex cavity begins to form just upstream of the trailing edge. Shortly thereafter, around ϕ=130° (point B), a few travelling bubbles may be seen near the leading edge. Some of these collapse quickly or are swept downstream, but a small number adhere to the leading edge itself and begin to elongate in the downstream direction. (The photograph in Figure 10 labelled "B/C" illustrates this stage of the cavity development.) Soon these attached bubbles coalesce into a single attached cavity (point C). The cavity is mostly clear and smooth except for a few specks of froth in the closure region. (This is shown in a slightly more advanced state in photograph "D" of Figure 10.) Often, these frothy regions occur where two bubbles have just coalesced while forming

the cavity, suggesting some link between the coalescence and the initial breakdown into bubbles.

Another interesting feature often evident in the cavity is a crescent-shaped area in the closure region, seen in the photos labelled "G" and "E" in Figure 10. It appears to "enclose" the frothy regions — that is, it curves smoothly into the froth — but it is not immediately evident whether this crescent is filled with vapor or with reentrant flow. Further study, in particular viewing the cavity from other angles, will be necessary in order to understand the role of this crescent in the cavitation process.

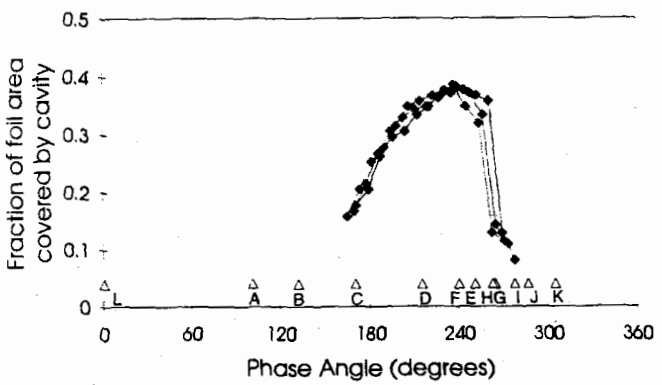

FIGURE 2. CAVITY SIZE PLOTTED AGAINST PHASE ANGLE, FOR REDUCED FREQUENCY k=0.73 AND CAVITATION NUMBER σ=1.34.

The cavity continues to grow in size as the angle of attack increases. At point D, it has reached its maximum extent along the leading edge of the foil, but it continues to extend downstream; Point F indicates the phase angle at which it attains its maximum projected area. The frothy regions propagate towards the center of the cavity; in particular, the bubbly regions closer to the tip of the foil move towards the base and those near the base shift towards the tip. The usual result is one large frothy area, located in a region of the foil around the center chord position, at about one-third span from the base. This stage is sketched by Bark and van Berlekom [1978] for several values of k (with σ = 0.76). From within this bubbly portion of the cavity, a sub-section of the froth may begin to protrude (point E, see also photograph "E" in Figure 10), often sending out tendrils of bubbly vortex loops that make it look like a tangled ball of string. Depending on the flow parameters this "subcloud" may be any shape, from nearly spherical (as in the "ball of string" formation) to almost indistinguishable from the main cavity.

Meanwhile, the smooth leading-edge portion of the cavity takes on a striated appearance, and shortly thereafter begins to detach from the leading edge (point G), beginning at the corner of the cavity closest to the foil tip. By this time the subcloud is usually fully detached from the frothy region (point H), and has begun to convect downstream. The remainder of the cavity then collapses into a second cloud (point I; see also photograph "I" in Figure 10), which is generally less coherent than the subcloud, and is swept downstream following the last traces of the collapsed subcloud. In some cases, the cloud generated by the collapse of the main cavity disappears while the subcloud is still extant (point J). Meanwhile, the tip vortex cavity, which had become thick as the cavity was growing, now begins to elongate and become thinner, and soon detaches (marked by point K; corresponding photograph "K" in Figure 10 shows the subcloud nearly at the trailing edge of the foil at this point). The two cloud collapses may occur nearly simultaneously, or at clearly distinct points in the oscillation cycle, depending on the conditions of the flow. When they collapse separately, the acoustic signature may reflect this by showing two distinct sound bursts in the collapse region of the cycle (see next section). Finally, point L indicates the phase angle at which the foil surface becomes completely clear of bubbles. The cycle then repeats itself.

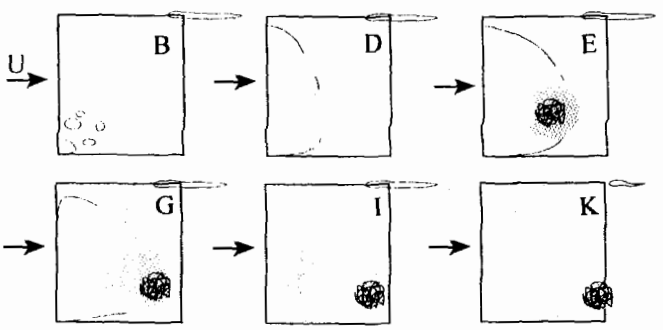

FIGURE 3. SCHEMATIC REPRESENTATION OF SELECTED EVENTS IN A TYPICAL CAVITATION CYCLE. SEE FIGURE 10 FOR PHOTOGRAPHS.

For the purposes of the present measurements, the cavity was considered not to exist until the initial travelling bubbles and isolated small attached cavities finished coalescing into a single coherent cavity attached to the leading edge. Then, when the cavity began to break up during the collapse phase, the whole projected area of cavity and froth was counted in the cavity area until the subcloud was fully detached, at which point the "cavity size" was considered to include only the remaining attached cavity but not the subcloud. Thus the cavity area will tend to decrease suddenly when the subcloud breaks off.

In Figure 4, cavity size plots for four different cavitation numbers show how the cavity size, and the growth process itself, change with cavitation number. The reduced frequency for all four cases is approximately k=0.74. As might be expected, the maximum cavity size increases as

the cavitation number is decreased, but it is also interesting to note how the shapes of the curves change with σ. In all cases, a single coherent attached cavity is achieved at approximately the same phase angle, but the maximum cavity area occurs much later for the lower cavitation numbers. At σ=1.34, the cavity size decreases rapidly during collapse as a result of the formation and breakoff of a large subcloud. In contrast, no distinct subcloud was observed at σ=1.53. Furthermore, at the two lowest cavitation numbers (σ=0.88 and σ=1.15) there is a marked, sudden increase in the cavity area just before the maximum is reached. This seems to mark the beginning of an explosive pre-collapse phase.

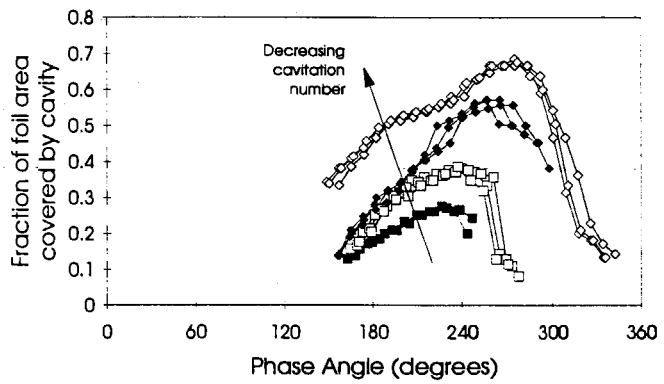

FIGURE 4. CAVITY AREA PLOTTED AGAINST PHASE ANGLE, FOR REDUCED FREQUENCY *k*=0.74 AND FOUR CAVITATION NUMBERS.
(■ σ=1.53, □ σ=1.34, ◆ σ=1.15, ◇ σ=0.88)

Figure 5 presents the average phase angles at which the identified events occur during the cavitation cycle, and shows how those occurrence times change with cavitation number. In general, the changes are not surprising. At lower σ, the cavitation (including the tip vortex cavity) tends to begin earlier and to last longer. In a few cases, however, there is unexpectedly little variation with σ. For example, while travelling bubble cavitation occurs earlier at lower cavitation numbers, the point at which it coalesces into a single coherent cavity attached to the leading edge is reasonably constant, as is the phase angle at which the cavity first reaches its maximum extent along the leading edge. There is also remarkable consistency in the phase angle at which the subcloud (for cases where one appears) first becomes clearly discernible.

One motion picture sequence was taken at a lower reduced frequency. Figure 6 compares the cavity size variations for the two different reduced frequencies at the same cavitation number. Event times are included in the figure in order to illustrate how they changed with reduced frequency. It is interesting to note that the cavity size increases only slightly for the lower reduced frequency, and it begins and ends at nearly the same phase angle. The shapes of the curves, however, are strikingly different for the two values of k shown. On the k=0.56 curve, beginning at point D (the point in the cycle where the cavity has reached its maximum extent along the leading edge of the foil), the cavity area suddenly increases sharply as the cavity expands in the downstream direction. Examining the movie footage it appears that, unlike the k=0.74 case where the froth is mostly contained within the smooth curve of the closure region, the k=0.56 cavity has froth that extends beyond the basic cavity shape, reaching downstream and sometimes even ejecting a few bubbly vortex tendrils before breaking off a large subcloud. For these conditions, it appears that the frothy, collapsing portion of the cavity reaches further upstream before the main cavity begins to detach from the leading edge (see relative positions of events G and H), in contrast to the higher reduced frequency case where the cavity detaches from the leading edge and collapses to meet the frothy region. The end product of this collapse is two clouds; the large subcloud and the cloud-like remains of the collapsed main cavity are both convected downstream and dissipate at approximately the same rate.

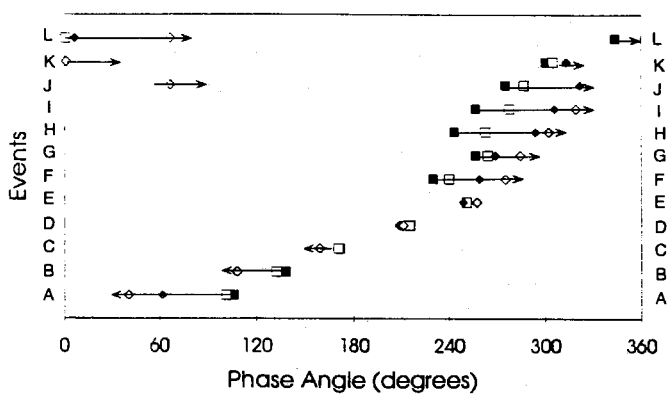

FIGURE 5. PHASE ANGLES OF SELECTED EVENTS IN CAVITATION CYCLE, FOR REDUCED FREQUENCY K=0.74 AND FOUR CAVITATION NUMBERS. (■ σ=1.53, □ σ=1.34, ◆ σ=1.15, ◇ σ=0.88)

In addition, it should be noted that nearly all the events indicated by the letters in the figure may be seen to occur later for the lower reduced frequency, not only those associated with the growth of the cavity but also those associated with its collapse. (The only exception to this pattern is event H indicating the breakoff of the subcloud, which occurs earlier due to the collapse of the main cavity as described above.) This is in striking contrast to the changes with cavitation number shown in Figure 5, where the cavitation process began earlier for decreasing cavitation number, but ended later. Changes in the process

with decreasing cavitation number, then, seem to be guided by the greater tendency toward cavitation; changes with decreasing reduced frequency, however, appear to be driven more by the phase lag introduced by the coupling of the fluid with the oscillation of the foil.

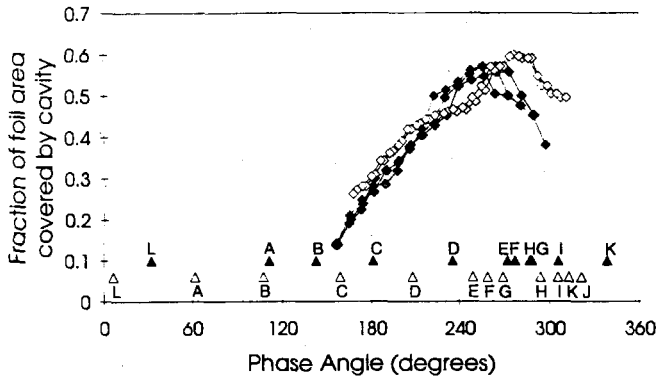

FIGURE 6. CAVITY SIZE PLOTTED AGAINST PHASE ANGLE, FOR CAVITATION NUMBER σ=1.15 AND TWO REDUCED FREQUENCIES.
(△ k=0.56, △ k=0.74)

CAVITATION ACOUSTICS

The violence with which cavitation collapses is well documented (Bark & van Berlekom, 1978; Kato, 1985; Ye, et al., 1989; Soyama, et al., 1992), and, in fact, the noise is readily apparent to the most casual visitor to the facility. Figure 7 shows typical raw data from a single oscillation cycle of the hydrofoil for the conditions noted in the caption. Even without filtering out the various mechanical resonances inherent in the facility, some of the features of the cavitation noise are evident. Standing out from the background noise, a large high-amplitude, high-frequency burst may be seen between phase angles of 340° and 355°; that is, in the last 3% of the oscillation cycle, just before the foil returns to zero angle of attack. Less prominent, but still visible, is a low-amplitude high-frequency burst at around ϕ=130°, where the angle of attack is about 8° and increasing. Using a digital high-pass filter algorithm most of the non-cavitation noise was then filtered out of the data, resulting in signals such as the one that appears in Figure 9.

The acoustic signals were analyzed in two ways. First, the overall "noise level", or *acoustic intensity*, was calculated for each set of conditions, in order to gain a perspective on the variations of the noise with reduced frequency and cavitation number. Second, the shapes of the individual signals were correlated with high speed motion pictures of the cavitation, in the hopes of identifying features in the cavity growth and collapse process which are responsible for the various features in the acoustic signature.

The measured acoustic intensity, p_A, is defined as

$$p_A = \frac{1}{T}\int (\overline{P} - P(t))dt,$$

and a dimensionless intensity is then defined by

$$p_A^* = \frac{p_A \ell}{\frac{1}{2}\rho U^2 c},$$

where ℓ is the distance from the cavitation to the hydrophone, ρ is the density of water, U is the freestream velocity, and c is the foil chord length.

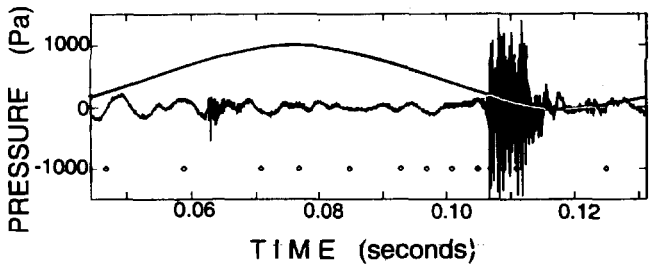

FIGURE 7. RAW ACOUSTIC SIGNAL FROM HYDROPHONE, FOR ONE CYCLE WITH CAVITATION NUMBER σ=1.15 AND REDUCED FREQUENCY k=0.74.

The quantity p_A^* provides a normalized measure of the strength of the noise produced by the cavitation. Figure 8 shows how this variable changed with reduced frequency, for three different values of cavitation number. (Here it should be noted that the acoustic intensity was calculated using unfiltered data, thus certain features may be related to increasing background noise and not to the cavitation itself.) The peaks in acoustic intensity corresponded very consistently with conditions under which the cavitation was heard to make a loud report or "bang" during collapse.

Each curve in Figure 8 contains two peaks, marked with arrows. As the reduced frequency increases, the value of the acoustic intensity is seen to increase, then decrease, then increase again; this may be related to a qualitative change in the cavity collapse process for certain ranges of reduced frequency. These peaks tend to increase in magnitude, and, for the cavitation numbers shown, also appear to shift toward lower reduced frequencies, with decreasing cavitation number.

The presence of two peaks may result from qualitative changes in the type of cavitation. As an example, between the cavitation numbers of about 1.3 and 1.5, there are distinct changes in the cavitation. The size of the cavity increases by almost 100% (from 1/4 chord to 1/2 chord) as the cavitation number is reduced, and the "ball of string" subcloud formation now appears during the collapse phase, detaching from the main cavity and travelling separately downstream. This is in contrast to the higher cavitation number process, where the cavity collapses into

a crescent-shaped frothy region which dissipates quietly. At the lower cavitation numbers (depending on reduced frequency) a "bang" can be heard as the cavitation collapses, suggesting that the existence of a distinct subcloud during collapse may be associated with the "bang". The higher cavitation number sequence does sometimes evidence tangled vortex tendrils within the frothy region, but there is no clear detachment of a separate formation. This would satisfactorily explain the very low acoustic intensities for σ=1.45 as shown in the figure.

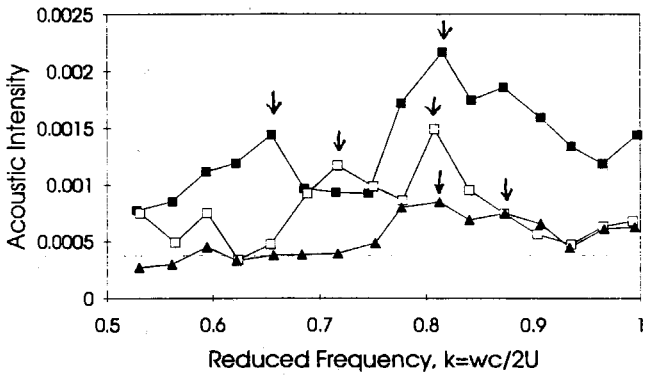

FIGURE 8. CHANGES IN ACOUSTIC INTENSITY, P_A^*, WITH REDUCED FREQUENCY FOR THREE CAVITATION NUMBERS. (▲ σ=1.45, □ σ=1.16, ■ σ=0.85)

The acoustic signals were also compared with the results obtained from the motion picture sequences. Figure 9 shows an oscillation cycle from one of the five cases examined (the acoustic data here has been high-pass filtered as described earlier), along with a curve showing the corresponding cavity area for the same cycle. Event times are also indicated. The distance between markers on the cavity area curve represents the time between one movie frame and the next (approximately 2 msec). The time required for the cavitation sound to travel from the trailing edge of the foil to the hydrophone is approximately 1/6 of the time between frames, which, on the scale of the graph, is negligible. Thus the fact that the main burst in the acoustic signal begins at the same phase angle as event I (see corresponding photo in Figure 10) means that the collapse of the cavity itself does not seem to contribute directly to the noise produced by the cavitation. In fact, the cavity size curve clearly shows that the main cavity ceases to exist as a coherent attached cavity almost as soon as the burst begins. The events contained within the main burst are I, K, and J: main cavity turned to froth, tip vortex cavity detached, and main cavity dissipated leaving subcloud, respectively. Since it is unlikely that the detachment of the tip vortex is a major contributor to the acoustic signal, we are forced to conclude that it is the process of dissipation of the main cavity froth that creates the major burst of noise in this cycle. This agrees with the observation of Shen and Peterson that "the peak amplitude of the noise occurs after the sheet cavitation has disappeared", and indeed they make the same conclusion about the source of the noise. At point J the main cavity is completely gone, leaving only the subcloud visible; the remaining portion of the burst thus may correspond to the subcloud beginning to collapse as it is swept to the trailing edge of the foil. Note that the subcloud does not fully clear the trailing edge until point L, but that the burst amplitude drops off as the foil again nears zero angle of attack.

The source of the smaller high-frequency burst, occurring just after ϕ=120°, is less easily discerned. Unfortunately the resolution of the high-speed movies is not sufficient to determine unequivocally what action in the cavitation caused the noise; one movie frame occurs just before the middle of the burst, the other just after the burst ends. The only change between the two frames is the disappearance of a few travelling bubbles on the surface of the foil. This leads to the speculation that the collapse of some of those travelling bubbles may have generated this small burst.

RESULTS AND CONCLUSIONS

It has been tentatively established that the primary burst in the acoustic signal corresponds not to the visually more striking sheet cavity collapse but rather to the collapse of the cloud cavitation which is formed later in the cycle. This suggests that the flow mechanisms contained in the cloud cavitation are indeed a significant factor in the noise generated by the cavitation process.

ACKNOWLEDGMENTS

This research is supported by the Office of Naval Research, contract number N00014-91-J-1295. Thanks also to undergraduate assistant Amit Mehra for his data reduction work.

REFERENCES

Bark, G., and van Berlekom, W. B., 1978. "Experimental investigations of cavitation noise." *Proc. of the Twelfth Symp. on Naval Hydrodynamics*, pp. 470–493.

Franc, J. P., and Michel, J. M., 1988. "Unsteady attached cavitation on an oscillating hydrofoil." *J. of Fluid Mech.*, Vol. 193, pp. 171–189.

Hart, D. P., Brennen, C. E., and Acosta, A. J., 1990. "Observations of cavitation on a three-dimensional oscillating hydrofoil." *Cavitation and Multiphase Flow Forum*, ASME FED Vol. 98, pp. 49–52.

Kato, H., Takasugi, N., and Yamaguchi, H., 1992. "Numerical analysis of a cavitating hydrofoil with finite span." Presented at the International Symposium on Propulsors and Cavitation, Hamburg, Germany, June 1992.

Kato, H., 1985. "On the structure of cavity — New insight into the cavity flow: A summary of the keynote speech." *Proc. of the International Symp. on Jets and Cavities*, ASME Vol. 31, pp. 13–19.

Kubota, A., Kato, H., Yamaguchi, H., and Maeda, M., 1989. "Unsteady structure measurement of cloud cavitation on a foil section using conditional sampling technique." *J. Fluids Eng.*, Vol. 240, pp. 59–96.

Kubota, A., Kato, H., and Yamaguchi, H., 1992. "A new modelling of cavitating flows: a numerical study of unsteady cavitation on a hydrofoil section." *J. of Fluid Mech.*, Vol. 111, June 1989, pp. 204–210.

Maeda, M., Yamaguchi, H., and Kato, H., 1991. "Laser holography measurement of bubble population in cavitation cloud on a foil section." *Cavitation '91*, ASME FED Vol. 116, pp. 67–75.

Shen, Y. T., and Peterson, F. B., 1980. "The influence of hydrofoil oscillation on boundary layer transition and cavitation noise." *Proc. of the Thirteenth Symp. on Naval Hydrodynamics*, pp. 221–241.

Shen, Y. T., and Peterson, F. B., 1978. "Unsteady cavitation on an oscillating hydrofoil." *Proc. of the Twelfth Symp. on Naval Hydrodynamics*, pp. 362–384.

Soyama, H., Kato, H., and Oba, R., 1980. "Cavitation observations of severely erosive vortex cavitation arising in a centrifugal pump." *Proc. of the IMechE Intl. Conf. on Cavitation*, Cambridge, England, pp. 103–111.

Ye, Y. P., Kato, H., and Maeda, M., 1989. "On correlation of cavitation erosion and noise on a foil section." Presented at the International Workshop on Cavitation, April 1989, China Ship Scientific Research Center, pp. 68–75.

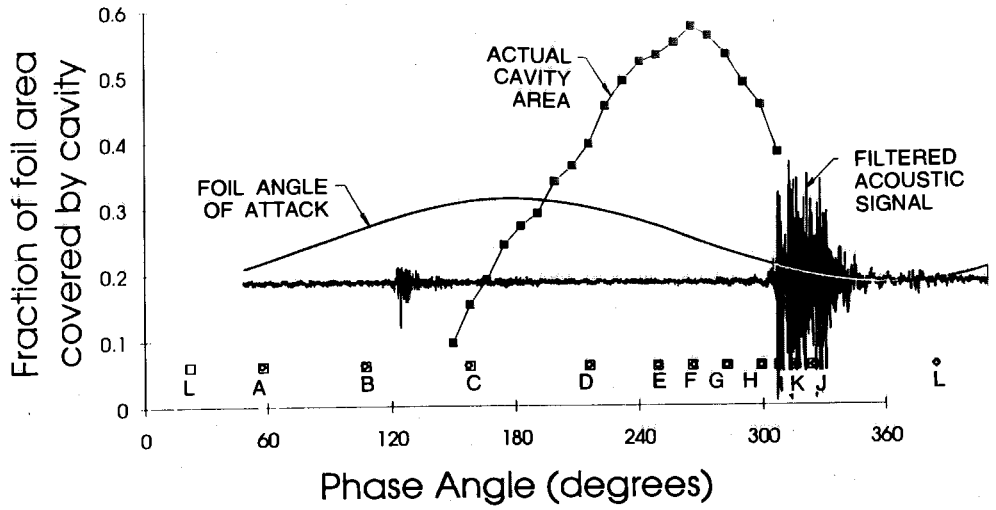

FIGURE 9. ACOUSTIC SIGNAL (HIGH-PASS FILTERED) FOR ONE OSCILLATION CYCLE, WITH EVENTS AND CORRESPONDING CAVITY SIZE. REDUCED FREQUENCY k=0.74, CAVITATION NUMBER σ=1.15.

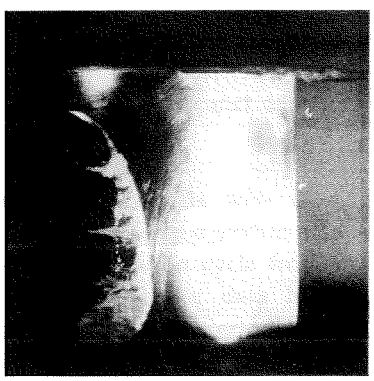

D. (σ = 1.15, k = 0.74)

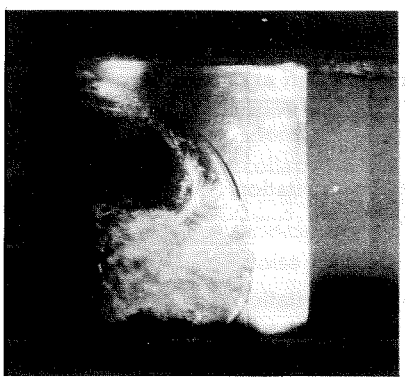

G. (σ = 1.15, k = 0.74)

I. (σ = 1.15, k = 0.74)

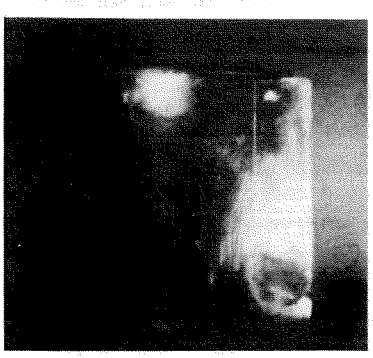

K. (σ = 1.15, k = 0.74)

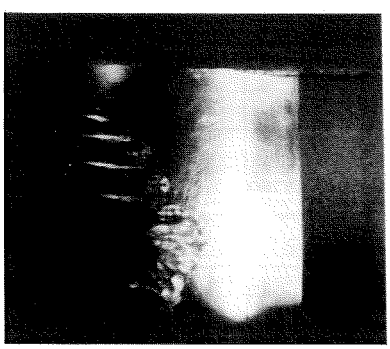

B/C. (σ = 0.88, k = 0.75)

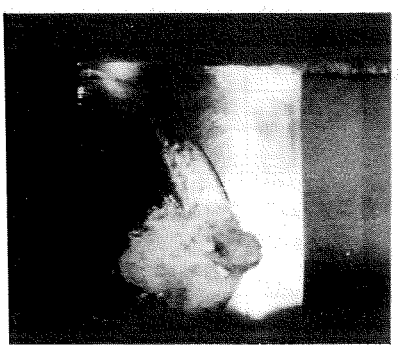

E. (σ = 0.88, k = 0.75)

FIGURE 10. MOTION PICTURE FRAMES CORRESPONDING WITH ACOUSTIC SIGNAL.